FULL PAPER

Pyridazine-Supported Polymeric Cyanometallates with Spin Transitions

Il'ya A. Gural'skiy,*[ab] Sergii I. Shylin,[ac] Vadim Ksenofontov,[c] and Wolfgang Tremel[c]

Abstract: Heterometallic cyano-bridged spin-crossover complexes form a large family of switchable compounds with different structural motives and diverse transition characteristics. Here we report on the hysteretic water dependent spin transitions found in the family of $[Fe(pyridazine)_2M(CN)_4]$ frameworks (M = Ni, Pd, Pt). The structure of three new spin-crossover compounds is built of cyanometallic layers supported by pyridazine ligands. The frameworks contain water guest molecules that can be removed upon heating. Spin transition was found in both hydrated and dehydrated compounds, while the removal of water stimulated a complete spin state switch. Mössbauer spectroscopy revealed two different high-spin centres in hydrated frameworks, and only one of them is switchable. The compounds display a pronounceable thermochromism, changing their colour from red in low-spin to yellow in high-spin. The work shows a perspective of 1,2-diazine application for the design of switchable complexes.

Introduction

Among the different phase transition materials, spin-crossover (SCO) compounds attract attention by their synthetic variability originating from a large set of inorganic/organic ligands suitable for the construction of SCO complexes of $3d^4$–$3d^7$ metals (mostly represented by iron(II) compounds). This provides molecular, 1D, 2D and 3D motives with practically any desired transition temperature, hysteresis, abruptness and completeness of the SCO, whose spin state can be communicated by means of temperature change, pressure, light irradiation, magnetic field or guest inclusion.[1–3] SCO complexes can be processed to different functional materials: nanoparticles,[4–8] thin films,[9–12] surface motives,[13,14] composites,[15,16] gels,[17–20] etc.

Cyanoheterometallates, considered as analogues of Hofmann chlathrates,[21] constitute a large family of Fe(II) SCO complexes including diverse spin transition compounds.[22] Their principal motif includes heterometallic cyano-bridged units supported by organic N-donor aromatic ligands. Cyano-units that were recruited may contain Ni, Pd, Pt, Cu, Ag, Au, Nb, etc.[22]; organic ligands are pyridines,[23] pyrazines,[24] pyrimidines[25] and triazoles[26]. The structure of an organic ligand strongly effects the structure and SCO properties of cyanometallic frameworks. 2,6-Naphthyridine Fe-Ag complex displays a spin transition at low temperatures,[27] while its isomer, 1,6-naphthyridine, leads to a compound that has a spin transition centred at room temperature.[28]

Diazines are among the most promising organic blocks for the construction of Fe(II) SCO heterocyanometallates. Complexes with pyrazines and pyrimidines are known for high temperature spin transitions,[29,30] pronounceable guest effects,[31,32] advanced crystal structures,[25] etc. The complex $[Fe(pz)Pt(CN)_4]$ has received much attention because it displays a room temperature spin transition and the compound is easily available synthetically.[24] Substituted diazines (5-bromopyrimidine[33] and chloro-, iodo- and methylpyrazines[34]) also offer pathways to numerous SCO analogues of the Hofmann clathrates. Pyridazine (1,2-diazine, *pdz*) is one of three diazines (with pyrimidine and pyrazine), which was recruited here to build new switchable SCO cyanometallates.

Results and Discussion

We have obtained three new frameworks $[Fe(pdz)_2M(CN)_4]$ by the reaction of $Fe(ClO_4)_2$, *pdz* and $K_2[M(CN)_4]$ (M= Ni, Pd, Pt). The complexes were produced as hydrates **1·H₂O** (Ni), **2·H₂O** (Pd), **3·H₂O** (Pt). After heating at 373 K for 5 min the dehydrated complexes were obtained: **1** (Ni), **2** (Pd), **3** (Pt).

The three frameworks **1·H₂O**, **2·H₂O** and **3·H₂O** are isostructural and crystallize in the orthorhombic space group *Cmmm*. Their typical crystal structure is shown in **Figure 1** (Pd complex).

The crystal structures contain metal-cyanide layers within the *ac*-plane. They are supported by N-coordinated *pdz* molecules. Palladium stays in square-planar environment as in the precursor, iron adopts a pseudo-octahedral coordination geometry. The cyanide ligands occupy the equatorial positions, and the axial positions of Fe atoms are filled by *pdz* ligands with aromatic moieties in the *bc*-plane. The *pdz* ligands are statistically disordered between two positions (C2/N3 50:50). The water molecules are also statistically disordered and located in voids of the framework with one H_2O molecule per Fe centre.

For all three complexes, the crystal structures were determined for both LS and HS states. The major changes upon spin

[a] Dr. I.A. Gural'skiy, Dr. S.I. Shylin
Department of Chemistry
Taras Shevchenko National University of Kyiv
Volodymyrska St. 64/13, Kyiv 01601, Ukraine
E-mail: ilia.guralskyi@univ.kiev.ua
Homepage: www.physchem.univ.kiev.ua/fritsky/guralskyi_eng.html
[b] Dr. I.A. Gural'skiy
UkrOrgSyntez Ltd.
Chervonotkatska St. 67, Kyiv 02094, Ukraine
[c] Dr. S.I. Shylin, Dr. V. Ksenofontov, Prof. W. Tremel
Institute of Inorganic and Analytical Chemistry
Johannes Gutenberg University of Mainz
Staudingerweg 9, Mainz 55099, Germany

Supporting information for this article is given via a link at the end of the document.

Table 1. Selected crystallographic information for **1·H₂O**, **2·H₂O** and **3·H₂O** in LS and HS states.

Complex	**1·H₂O**		**2·H₂O**		**3·H₂O**	
Spin state	HS (243 K)	LS (173 K)	HS (296 K)	LS (153 K)	HS (296 K)	LS (153 K)
R_1 (%)	5.70	2.41	2.85	2.97	1.65	1.12
a (Å)	7.222(3)	6.9234(15)	7.365(9)	7.0729(13)	7.401(2)	7.0858(9)
b (Å)	15.172(7)	14.676(3)	14.969(18)	14.583(3)	15.058(5)	14.5878(18)
c (Å)	7.433(3)	7.1195(15)	7.538(9)	7.2986(13)	7.538(2)	7.2887(9)
V (Å^3)	814.5(6)	723.4(3)	831.0(17)	752.8(2)	840.1(5)	753.41(16)
Fe-N1	2.145(5)	1.948(3)	2.155(3)	1.943(3)	2.144(3)	1.942(2)
Fe-N2	2.207(6)	1.982(3)	2.202(5)	1.996(5)	2.217(4)	1.989(3)
N1-Fe-N1i	91.1(2)	90.41(14)	90.81(16)	90.48(17)	90.44(19)	90.70(12)
V_{oct}(FeN$_6$)	13.534	10.029	13.639	10.051	13.598	10.000
Σ(N-Fe-N)	4.4	1.64	3.24	1.92	1.76	2.8
π-π	3.611	3.4617	3.683	3.5365	3.701	3.543
O1···N3	2.871	2.729	2.858	2.780	2.845	2.768

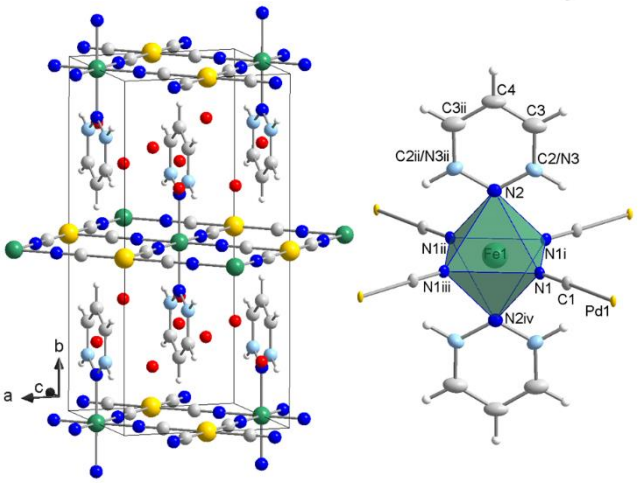

Figure 1. Crystal structure of **2·H₂O**. Framework consists of Fe-Pd cyano-bridged layers supported by monocoordinated *pdz* ligands (left). Iron ions are located in N_6 coordination environment of four cyanides and two *pdz* (right). Elements: Fe (green), Pd (yellow), C (gray), N (blue), C/N (cyan), O (red). Symmetry operations: (i) 1-x, 1-y, 1/2; (ii) 1-x, y, 1-z; (iii) x, 1-y, 1-z; (iv) 1-x, 1-y, z.

transition derive from the Fe-N bond length variation, which is mostly related to the transfer of electrons between nonbonding t_{2g} and antibonding e_g orbitals (**Table 1**).

The Fe-N bond length for the cyanide ligand is shorter compared to the pyridazine heteroatom. The medium Fe-N1 (of CN) bond length is in the range 1.94-1.95 Å in the LS sate and it growths to 2.14-2.16 Å in the HS state. The same tendency is observed for the Fe-N2 (of *pdz*) bond length: in the LS state it is 1.98-2.00 Å, while it reaches 2.20-2.22 Å in the HS state. This bond length change of ~10% is responsible for the expansion of FeN_6 polyhedron upon LS→HS transition: in the LS state the octahedron volume is ~10 Å^3, in the HS state it is of 13.5-13.6 Å^3. This change of volume around Fe is transmitted to the frameworks and leads to an expansion (LS→HS) / contraction (HS→LS) of the lattice in all directions. The lattice volume changes upon the LS→HS transition by 12.6 % (**1·H₂O**), 10.4 % (**2·H₂O**) and 11.5 % (**3·H₂O**). Due to the small size of the organic ligands the observed expansions are among the largest reported for the SCO.[16]

There is a weak π-π stacking between pyridazine ligands which is dependent on the spin state of the complex. The plane to plane distance is equal to a half cell parameter *a*. The inter-plane (*pdz* to *pdz*) distance is 3.46-3.54 Å in the LS state and 3.61-3.70 Å in the HS state. This weakening of the stacking is thus related to the general expansion of the framework. The same tendency is observed for hydrogen bonding: O1···N3 distance drops from 2.85-2.87 Å in the HS structures to 2.73-2.78 Å in the LS structures. This supramolecular arrangement into a 3D framework via hydrogen bonding is present in all three hydrated structures.

Magnetic measurements show that all three frameworks display a spin transition upon heating/cooling (**Figure 2**). The transition temperatures are given in **Table 2**. At room temperature the frameworks are paramagnetic and have $\chi_M T$ values of 3.4-3.5 cm^3

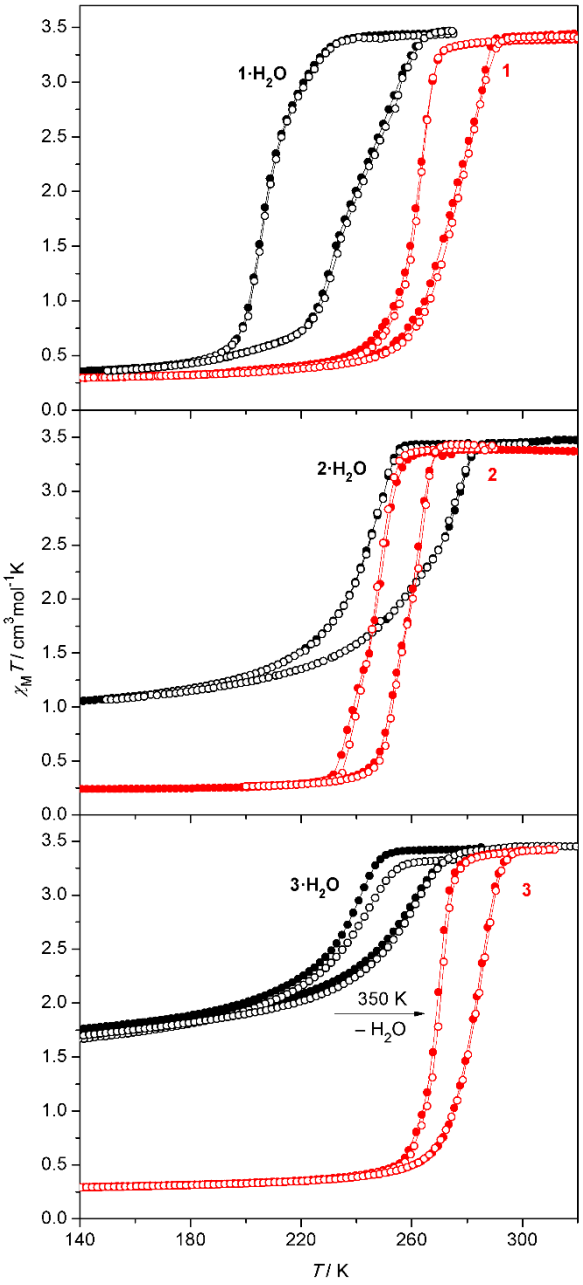

Figure 2. Hysteretic spin transitions in the family of [Fe(*pdz*)$_2$M(CN)$_4$] complexes (M = Ni, Pd, Pt). Hydrated frameworks display incomplete spin transitions, whereas dehydrated complexes show complete cooperative spin transitions at higher temperatures. 1st cycle – filled circles, 2nd cycle – open circles.

mol^{-1} K that are within a typical range for HS Fe(II) complexes. Upon cooling, this value gradually drops to ~ 0.4 (**1·H$_2$O**), 1.1 (**2·H$_2$O**) and 1.7 cm^3 mol^{-1} K (at 140 K) that corresponds to non-complete (especially, for **2·H$_2$O** and **3·H$_2$O**) spin transitions. These residual fractions at low temperature appear because not all spin centres undergo temperature-induced SCO. This should be explained by the loss of hydrogen bonding which is present in hydrated samples and indirectly effects the spin state of Fe centres. These fractions are reflected by the Mössbauer spectra of **1·H$_2$O**-**3·H$_2$O** (**Figure 3**) which show the presence of two HS components that differ by a quadrupole splitting.

Table 2. Spin transition temperatures for the hydrated and dehydrated complexes **1**–**3**.

Complex	$T\uparrow$ (K)	$T\downarrow$ (K)	ΔT (K)
[Fe(*pdz*)$_2$Ni(CN)$_4$]·H$_2$O (**1·H$_2$O**)	240	208	32
Fe(*pdz*)$_2$Ni(CN)$_4$] (**1**)	276	262	14
[Fe(*pdz*)$_2$Pd(CN)$_4$]·H$_2$O (**2·H$_2$O**)	265	242	23
[Fe(*pdz*)$_2$Pd(CN)$_4$] (**2**)	260	247	13
[Fe(*pdz*)$_2$Pt(CN)$_4$]·H$_2$O (**3·H$_2$O**)	255	235	20
[Fe(*pdz*)$_2$Pt(CN)$_4$] (**3**)	283	269	14

Their hyperfine parameters are summarized in **Table 3**. Centres corresponding to the first component (HS1) with δ = 1.04-1.05 mm s^{-1} and ΔE_Q = 1.1-1.4 mm s^{-1} (measured at 293 K) can undergo the SCO. The other centres are represented by the second component (HS2) with δ = 1.07-1.13 mm s^{-1} and ΔE_Q = 2.4-2.6 mm s^{-1} (at 293 K). They display no SCO and are HS within the whole temperature region.

Low-temperature (77 K) Mössbauer spectra of **1·H$_2$O**-**3·H$_2$O** (**Table 3**) show the presence of the non-SCO fraction (HS2) and the newly emerged LS fraction (δ = 0.41-0.44 mm s^{-1}, ΔE_Q = 0.17-0.23 mm s^{-1}). The increase of δ for HS2 upon cooling is due to the second-order Doppler shift, whereas the enhancement of ΔE_Q reflects a higher difference in the population of the d_{xy} and d_{xz}/d_{yz} levels at lower temperatures.

The presence of two different kinds of HS centres was not observed in our diffraction experiments, while this may be an effect of the hydration degree or selected temperatures of experiments. This observation of a non-SCO fraction HS2 (detected by Mössbauer spectroscopy) also corroborates with the incomplete nature of SCO in **1·H$_2$O**-**3·H$_2$O** observed in the magnetic measurements and the elevated values of $\chi_M T$ at temperatures below the spin transition. This effect should be attributed to a strong cooperativity in single crystals of the complex stimulating a complete thermal SCO of hydrated samples.

A different behaviour is found for the dehydrated frameworks **1**-**3** (**Figure 2**). They display spin transitions at temperatures considerably higher than those of the hydrated complexes (**Figure 2**, **Table 2**). For example, the transition in **3** occurs at $T\uparrow$ = 283 K and $T\downarrow$ = 269 K. This makes this complex interesting for near room temperature experiments and applications. Moreover, while in pyridine analogues the spin transition occurs at low temperatures[35–37], these new examples show that 2D analogues of Hofmann clathrates also may have spin transitions at temperatures close to those of their 3D analogues.[24]

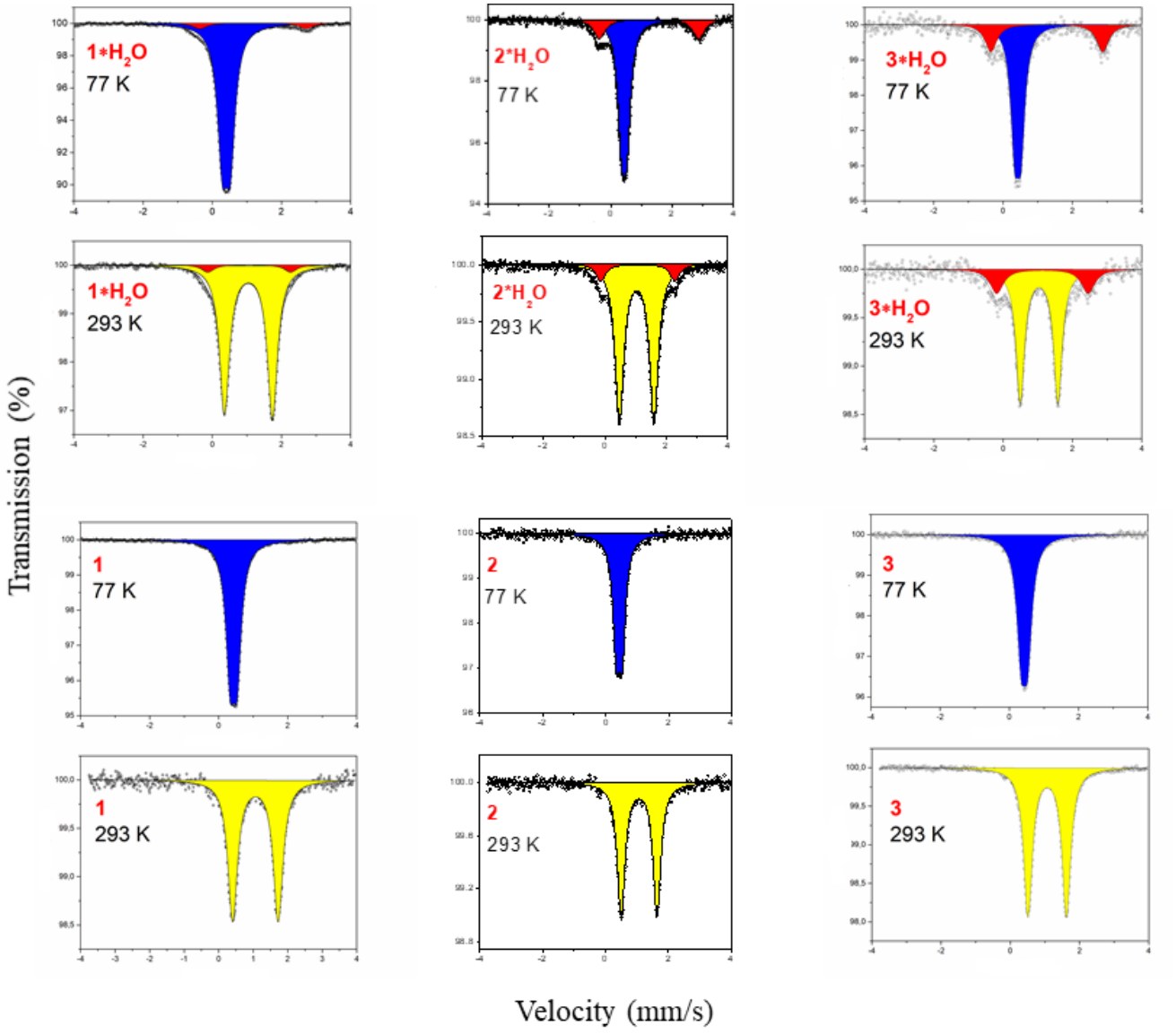

Figure 3. Mössbauer spectra of **1·H₂O**-**3·H₂O** and **1**-**3** at 77 and 293 K. Two HS fractions (HS1 and HS2) are observed at 293 K in hydrated samples. HS1 completely turns into LS fraction at 77 K, whereas HS2 stays unchanged. Dehydrated samples display a complete spin transition. Color codes: HS1- red, HS2 – yellow, LS- blue.

The SCO is complete for the dehydrated samples. At room temperature, $\chi_M T$ is of 3.3-3.5 $cm^3\ mol^{-1}\ K$. Upon the HS→LS spin transition it drops to 0.2-0.3 $cm^3\ mol^{-1}\ K$. Mössbauer spectra of **1**-**3** at room temperature (**Table 3**, **Figures 3**) show primarily one HS fraction (δ = 1.06-1.07 mm s^{-1}, ΔE_Q = 1.11-1.32 mm s^{-1}), which is completely transformed into the LS form at low temperatures (δ = 0.43-0.44 mm s^{-1}, ΔE_Q = 0.19-0.20 mm s^{-1}). Such difference in the behavior of hydrated and dehydrated samples cannot be described only in terms of cooperativity: while for all three complexes the thermal hysteresis of hydrated samples is larger, the transitions in dehydrated samples are more abrupt. Among the different switchable properties, thermochomism is a spectacular example that is typical for all SCO complexes, and it is proposed for applications in pure complexes, thin films, composites, etc.[38–42] We have selected the most spectacular representative among the three studied compounds – the platinum complex, which (in dehydrated form) displays molecular bistability near room temperature.

The complex **3** was dehydrated in a nitrogen atmosphere and its colour was monitored in the temperature range 243 – 303 K. The colour of the complex changes upon SCO similarly to most of the clathrates analogues. The compound is yellow in the HS form and changes its colour to intensively red upon transition to the LS state. Following the intensity of reflected light is a convenient way to monitor the spin transitions. The corresponding dependence of the reflectance with temperature is given in **Figure 4**. The

Table 3. Hyperfine Mössbauer parameters for the complexes of $[Fe(pdz)_2M(CN)_4]$ family (M = Ni, Pd, Pt) at 77 K and 293 K.

Complex	Spin state	77 K			293 K		
		δ (mm s^{-1})	ΔE_Q (mm s^{-1})	Cont. (%)	δ (mm s^{-1})	ΔE_Q (mm s^{-1})	Cont. (%)
1·H₂O	LS	0.406(1)	0.232(2)	94(1)	--	--	0
	HS1	--	--	0	1.052(1)	1.390(2)	95(1)
	HS2	1.176(2)	3.069(4)	6(1)	1.07(1)	2.4(2)	5(2)
1	LS	0.433(1)	0.202(2)	100	--	--	0
	HS1	--	--	0	1.068(3)	1.318(7)	100
2·H₂O	LS	0.441(2)	0.173(5)	79(1)	--	--	0
	HS1	--	--	0	1.037(2)	1.124(4)	85(3)
	HS2	1.25(1)	3.23(2)	21(2)	1.073(3)	2.405(6)	15(4)
2	LS	0.431(2)	0.188(4)	100	--	--	0
	HS1	--	--	0	1.062(3)	1.139(5)	100
3·H₂O	LS	0.43(1)	0.18(2)	75(2)	--	--	0
	HS1	--	--	0	1.037(3)	1.088(7)	77(2)
	HS2	1.26(2)	3.23(3)	25(3)	1.13(2)	2.64(5)	23(3)
3	LS	0.435(1)	0.189(3)	100	--	--	0
	HS1	--	--	0	1.067(1)	1.111(2)	100

transition temperatures extracted from the curve are $T\downarrow$= 265 K and $T\uparrow$ = 284 K, that correspond well to those in magnetic measurements. The minor difference is due to the thermalization conditions and particularly used sweep rates, which are different in optical (10 K/min) and magnetic (2 K/min) set-ups. In the optical experiment we observed a hysteresis loop of 4 K wider then in magnetic measurement. Such thermochromic changes near room temperature are interesting, especially considering the dependence of the described SCO on the water guest molecules. The DSC curves for the dehydrated complex **3** were obtained on heating and cooling in the 220 – 300 K temperature range. They show one endothermic peak on heating corresponding to the LS→HS transition and one exothermic peak on cooling corresponding to the HS→LS transition. The DSC peaks are centred at $T\downarrow$= 260 K and $T\uparrow$ = 278 K. The enthalpy changes calculated from the DSC curves are $\Delta H\downarrow$ = -16.4 KJ mol^{-1} and $\Delta H\uparrow$ = 13.5 KJ mol^{-1}. The corresponding entropy changes are $\Delta S\downarrow$ = -63.1 J mol^{-1} K^{-1} and $\Delta S\uparrow$ = 48.6 J mol^{-1} K^{-1}. Apart from the contribution to the entropy related to the spin change, there is also a major contribution from changes of lattice vibrations. These changes of enthalpy and entropy are within the typical range found for Fe(II) SCO complexes.

Conclusions

The pyridazine heterocycle is found capable to form analogues of Hoffman clathrates displaying spin transitions. This opens a route towards a new sub-class of SCO complexes with pyridazine and different cyanometallates. Importantly, more complex pyridazine-like ligands show now perspective for the design of cyanometallic switchable frameworks. Thus, substituted pyridazines, phtalazines and other 1,2-diazine heterocycles have potential for the design of SCO frameworks.

Spin transitions in these new compounds were found sensitive to the water inclusion. The spin transition upon loss of water molecules becomes complete and more abrupt, but the hysteresis width gets smaller. Importantly, Mössbauer spectroscopy allows to separately detect two kinds of HS iron(II) centres in a hydrated framework, those displaying thermal SCO and staying HS in the whole temperature range.

Abrupt spin transitions near room temperature as in **3** are rare and most looked for when new SCO compounds are studied. Moreover, a sensitivity to water effecting spin states of **3** near

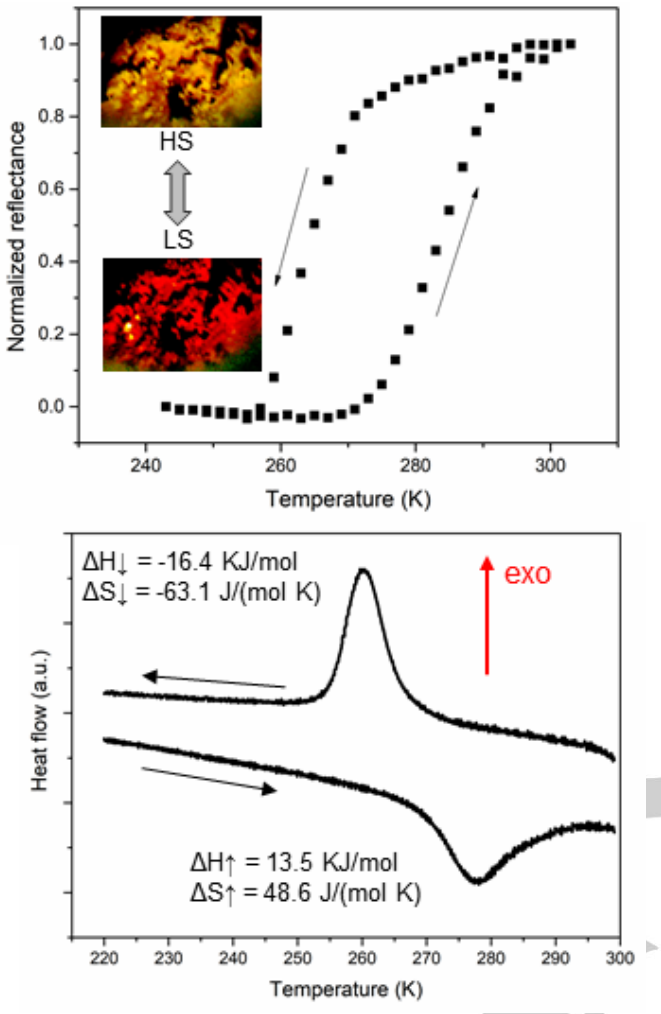

Figure 4. (up) Normalized change of the optical reflectivity for **3** vs. temperature. The change between red and yellow colours upon SCO can be monitored through optical microscopy. (down) DSC curves showing thermal effects of spin transitions in **3**. The extracted thermodynamic parameters are given for each peak.

room temperature makes this complex interesting for guest detection studies.

A considerable thermochromic effect accompanying these transitions can be used as an effective measure for the detection. These complexes with SCO-associated volume change, overcoming 12 % for **1**, may find application in constructing molecular actuators with a high work density of an active material. Simple frameworks reported here show the potential of azines, and especially diazines for building new SCO frameworks with attractive transition characteristics.

Experimental Section

Synthesis. In a typical experiment, $Fe(ClO_4)_2 \cdot 6H_2O$ (0.1 mmol) and *pdz* (0.5 mmol) in water (1 ml) were mixed with $K_2[M(CN)_4]$ (0.1 mmol) in water (1 ml). Yellow precipitates **1·H₂O-3·H₂O** were centrifuged off, washed with water and dried in air. Yields are 75-85 %. Dehydrated powders **1**-**3** were obtained by drying hydrated samples at 373 K for 5 min. Elemental analyses: for **1·H₂O** - calc. C 36.32%, H 2.54 %, N 28.24%, found C 36.23%, H 2.60 %, N 28.06%; for **2·H₂O** - calc. C 32.42%, H 2.27 %, N 25.21%, found C 32.77%, H 2.53 %, N 25.20%; for **3·H₂O** - calc. C 27.03%, H 1.89 %, N 21.02%, found C 26.58%, H 2.03 %, N 20.79%.

Crystallization. Crystals of **1·H₂O-3·H₂O** were obtained by a slow diffusion between $Fe(ClO_4)_2 \cdot 6H_2O$ (0.1 mmol) and *pdz* (0.5) in EtOH (2 ml) from one side and $K_2[M(CN)_4]$ (0.1 mmol) in water (2 ml) from another side through a H_2O-EtOH (50:50) layer (2 ml).

XRD measurements. Data for all structures were collected on a Bruker SMART diffractometer using Mo-Kα radiation. The structures were solved with the ShelXS using Direct Methods and refined with the ShelXL using Least Squares minimization.[43] Olex2 was used as an interface to ShelX programs.[44] All non-hydrogen atoms were refined using an anisotropic model. Hydrogen atoms of pdz were placed at calculated positions and refined using a riding model. CCDC deposition numbers are 1838583-1838588.

Magnetic susceptibility measurements. Temperature-dependent magnetic susceptibility measurements were carried out in a QuantumDesign MPMS-XL-5 SQUID magnetometer equipped with a 5 T magnet over the temperature range 140–320 K with a heating and cooling rate of 2 K min^{-1} and a magnetic field of 0.5 T. Diamagnetic corrections for the molecules were derived from the Pascal's constants.

Mössbauer measurements. ^{57}Fe-Mössbauer spectra were recorded in transmission geometry with a ^{57}Co source in a rhodium matrix using a conventional constant-acceleration Mössbauer spectrometer equipped with a nitrogen gas-flow cryostat. Isomer shifts are given with respect to an α-Fe foil at ambient temperature. Fits of the experimental Mössbauer data were performed using the Recoil software (Lagarec and Rancourt, Ottawa University).

Reflectivity and DSC measurements. The system for monitoring the spin transition by changing the intensity of the reflected light consisted of an optical microscope Optica SZM-1 equipped with a camera Sigeta UCMOS 1300. The sample temperature was controlled with a Linkam optical cryostat DSC600 at a heating/cooling rate of 10 K/min. Before starting experiment, the air was purged off from the stage chamber with dry nitrogen. Photographs were taken automatically using ToupView software (one image per degree). Image processing was performed using ImageJ software.

Acknowledgments

This work was supported by the H2020-MSCA-RISE-2016 Project 73422 and Projects DZ/55-2018 and 19BF037-01M from the Ministry of Education and Science of Ukraine.

Keywords: spin crossover • iron • pyridazine • cyanometallate • magnetism

[1] P. Gütlich, H. A. Goodwin, in *Top. Curr. Chem.*, Springer, **2004**.

[2] A. Bousseksou, G. Molnár, L. Salmon, W. Nicolazzi, *Chem. Soc. Rev.* **2011**, *40*, 3313.

[3] G. Molnár, S. Rat, L. Salmon, W. Nicolazzi, A. Bousseksou, *Adv.*

Mater. **2018**, *30*, 1–23.

[4] E. Coronado, J. R. Galán-Mascarós, M. Monrabal-Capilla, J. García-Martínez, P. Pardo-Ibáñez, *Adv. Mater.* **2007**, *19*, 1359–1361.

[5] J. Larionova, L. Salmon, Y. Guari, A. Tokarev, K. Molvinger, G. Molnár, A. Bousseksou, *Angew. Chemie Int. Ed.* **2008**, *47*, 8236–8240.

[6] T. Forestier, S. Mornet, N. Daro, T. Nishihara, S. Mouri, K. Tanaka, O. Fouché, E. Freysz, J.-F. Létard, *Chem. Commun.* **2008**, 4327–4329.

[7] F. Volatron, L. Catala, E. Rivière, A. Gloter, O. Stéphan, T. Mallah, *Inorg. Chem.* **2008**, *47*, 6584–6586.

[8] I. Boldog, A. B. Gaspar, V. Martínez, P. Pardo-Ibañez, V. Ksenofontov, A. Bhattacharjee, P. Gütlich, J. A. Real, *Angew. Chemie Int. Ed.* **2008**, *47*, 6433–6437.

[9] A. Pronschinske, Y. Chen, G. F. Lewis, D. A. Shultz, A. Calzolari, M. Buongiorno Nardelli, D. B. Dougherty, *Nano Lett.* **2013**, *13*, 130327091617008.

[10] D. Tanaka, N. Aketa, H. Tanaka, T. Tamaki, T. Inose, T. Akai, H. Toyama, O. Sakata, H. Tajiri, T. Ogawa, *Chem. Commun.* **2014**, *50*, 10074–10077.

[11] O. Roubeau, B. Agricole, R. Clérac, S. Ravaine, *J. Phys. Chem. B* **2004**, *108*, 15110–15116.

[12] H. Naggert, J. Rudnik, L. Kipgen, M. Bernien, F. Nickel, L. M. Arruda, W. Kuch, C. Näther, F. Tuczek, *J. Mater. Chem. C* **2015**, *3*, 7870–7877.

[13] C. Bartual-Murgui, A. Akou, L. Salmon, G. Molnár, C. Thibault, J. A. Real, A. Bousseksou, *Small* **2011**, *7*, 3385–3391.

[14] A. Akou, I. A. Gural'skiy, L. Salmon, C. Bartual-Murgui, C. Thibault, C. Vieu, G. Molnar, A. Bousseksou, *J. Mater. Chem.* **2012**, *22*, 3752–3757.

[15] T. Zhao, L. Cuignet, M. M. Dîrtu, M. Wolff, V. Spasojevic, I. Boldog, A. Rotaru, Y. Garcia, C. Janiak, *J. Mater. Chem. C* **2015**, *3*, 7802–7812.

[16] H. J. Shepherd, I. A. Gural'skiy, C. M. Quintero, S. Tricard, L. Salmon, G. Molnár, A. Bousseksou, *Nat. Commun.* **2013**, *4*, 2607.

[17] A. Sánchez-Ferrer, I. Bräunlich, J. Ruokolainen, M. Bauer, R. Schepper, P. Smith, W. Caseri, R. Mezzenga, *RSC Adv.* **2014**, *4*, 60842–60852.

[18] O. Roubeau, A. Colin, V. Schmitt, R. Clérac, *Angew. Chemie Int. Ed.* **2004**, *43*, 3283–3286.

[19] I. A. Gural'skiy, C. M. Quintero, G. Molnár, I. O. Fritsky, L. Salmon, A. Bousseksou, *Chem. Eur. J.* **2012**, *18*, 9946–9954.

[20] I. A. Gural'skiy, V. A. Reshetnikov, A. Szebesczyk, E. Gumienna-Kontecka, A. I. Marynin, S. I. Shylin, V. Ksenofontov, I. O. Fritsky, *J. Mater. Chem. C* **2015**, *3*, 4737–4741.

[21] K. A. Hofmann, F. Höchtlen, *Berichte der Dtsch. Chem. Gesellschaft* **1903**, *36*, 1149–1151.

[22] M. C. Muñoz, J. A. Real, *Coord. Chem. Rev.* **2011**, *255*, 2068–2093.

[23] T. Kitazawa, Y. Gomi, M. Takahashi, M. Takeda, M. Enomoto, A. Miyazaki, T. Enoki, *J. Mater. Chem.* **1996**, *6*, 119–121.

[24] V. Niel, J. M. Martinez-Agudo, M. C. Muñoz, A. B. Gaspar, J. A. Real, *Inorg. Chem.* **2001**, *40*, 3838–3839.

[25] V. Niel, A. L. Thompson, M. C. Muñoz, A. Galet, A. E. Goeta, J. A. Real, *Angew. Chemie Int. Ed.* **2003**, *42*, 3760–3763.

[26] F. J. Muñoz-Lara, A. B. Gaspar, M. C. Muñoz, A. B. Lysenko, K. V. Domasevitch, J. A. Real, *Inorg. Chem.* **2012**, *51*, 13078–13080.

[27] L. Piñeiro-López, F. J. Valverde-Muñoz, M. Seredyuk, C. Bartual-Murgui, M. C. Muñoz, J. A. Real, *Eur. J. Inorg. Chem.* **2018**, *2018*, 289–296.

[28] V. M. Hiiuk, S. Shova, A. Rotaru, V. Ksenofontov, I. O. Fritsky, I. A. Gural'skiy, *Chem. Commun.* **2019**, *55*, 3359–3362.

[29] I. A. Gural'skiy, B. O. Golub, S. I. Shylin, V. Ksenofontov, H. J. Shepherd, P. R. Raithby, W. Tremel, I. O. Fritsky, *Eur. J. Inorg. Chem.* **2016**, *2016*, 3191–3195.

[30] I. A. Gural'skiy, S. I. Shylin, B. O. Golub, V. Ksenofontov, I. O. Fritsky, W. Tremel, *New J. Chem.* **2016**, *40*, 9012–9016.

[31] M. Ohba, K. Yoneda, G. Agustí, M. C. Muñoz, A. B. Gaspar, J. A. Real, M. Yamasaki, H. Ando, Y. Nakao, S. Sakaki, et al., *Angew. Chemie Int. Ed.* **2009**, *48*, 4767–4771.

[32] G. Agustí, R. Ohtani, K. Yoneda, A. B. Gaspar, M. Ohba, J. F. Sánchez-Royo, M. C. Muñoz, S. Kitagawa, J. A. Real, *Angew. Chemie Int. Ed.* **2009**, *48*, 8944–8947.

[33] G. Agustí, A. B. Gaspar, M. C. Muñoz, J. A. Real, *Inorg. Chem.* **2007**, *46*, 9646–9654.

[34] O. I. Kucheriv, S. I. Shylin, V. Ksenofontov, S. Dechert, M. Haukka, I. O. Fritsky, I. A. Gural'skiy, *Inorg. Chem.* **2016**, *55*, 4906–4914.

[35] M. González M, H. Osiry, M. Martínez, J. Rodríguez-Hernández, A. A. Lemus-Santana, E. Reguera, *J. Magn. Magn. Mater.* **2019**, *471*, 70–76.

[36] T. Kitazawa, T. Kishida, T. Kawasaki, M. Takahashi, *Hyperfine Interact.* **2017**, *238*, 65.

[37] S. Sakaida, K. Otsubo, O. Sakata, C. Song, A. Fujiwara, M. Takata, H. Kitagawa, *Nat. Chem.* **2016**, *8*, 377–383.

[38] M. P. . Cuéllar, A. . Lapresta-Fernández, J. M. . Herrera, A. . Salinas-Castillo, M. D. C. . Pegalajar, S. . Titos-Padilla, E. . Colacio, L. F. . Capitán-Vallvey, *Sensors Actuators, B Chem.* **2015**, *208*, 180–187.

[39] I. Bräunlich, S. Lienemann, C. Mair, P. Smith, W. Caseri, *J. Mater. Sci.* **2015**, *50*, 2355–2364.

[40] A. D. . Naik, L. . Stappers, J. . Snauwaert, J. . Fransaer, Y. . Garcia, *Small* **2010**, *6*, 2842–2846.

[41] M. Seredyuk, A. B. Gaspar, V. Ksenofontov, S. Reiman, Y. Galyametdinov, W. Haase, E. Rentschler, P. Gütlich, *Chem. Mater.* **2006**, *18*, 2513–2519.

[42] A. Lapresta-Fernández, M. P. Cuéllar, J. M. Herrera, A. Salinas-Castillo, M. D. C. Pegalajar, S. Titos-Padilla, E. Colacio, L. F. Capitán-Vallvey, *J. Mater. Chem. C* **2014**, *2*, 7292–7303.

[43] G. M. Sheldrick, *Acta Crystallogr. Sect. C Struct. Chem.* **2015**, *71*, 3–8.

[44] O. V. Dolomanov, L. J. Bourhis, R. J. Gildea, J. A. K. Howard, H. Puschmann, *J. Appl. Crystallogr.* **2009**, *42*, 339–341.

Entry for the Table of Contents

FULL PAPER

Heterometallic cyano-bridged spin-crossover complexes form a large family of switchable compounds with different structural motives and diverse transition characteristics. Here we report on the hysteretic water dependent spin transitions found in the family of $[Fe(pyridazine)_2M(CN)_4]$ frameworks (M = Ni, Pd, Pt). The work shows a perspective of 1,2-diazine application for the design of switchable complexes.

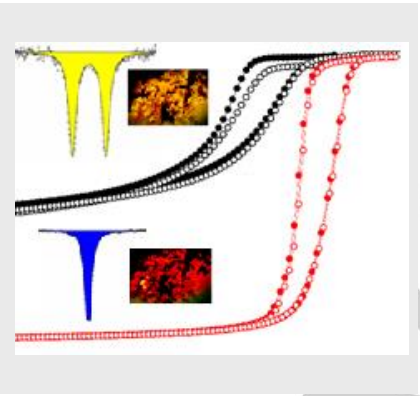

Spin Crossover

Il'ya A. Gural'skiy, Sergii I. Shylin, Vadim Ksenofontov, Wolfgang Tremel

Page No. – Page No.

Pyridazine-Supported Polymeric Cyanometallates with Spin Transitions